Supporting Information for

Toward Continuous Breath Monitoring on a Mobile Phone Using a Frugal Conducting Cloth-Based Smart Mask

Pillalamarri Srikrishnarka,[†,‡] Raaga Madhuri Dasi,[↕] Sourav Kanti Jana,[†] Tripti Ahuja,[†] Jenifer Shantha Kumar,[†] Ankit Nagar,[†] Amoghavarsha Ramachandra Kini,[†] Boby George[↕] and Thalappil Pradeep[*†]*

† DST Unit of Nanoscience and Thematic Unit of Excellence, Department of Chemistry, Indian Institute of Technology Madras, India 600036.

‡ Department of Chemical Engineering, Indian Institute of Technology Madras, India 600036.

↕ Department of Electrical Engineering, Indian Institute of Technology Madras, India 600036.

*E-mail: boby@iitm.ac.in, pradeep@iitm.ac.in

PS and DRM have contributed equally

SUPPORTING INFORMATION CONTENT

Total number of pages: 27

Total number of figures: 11

Total number of tables: 7

TABLE OF CONTENTS

Note S1. Volatile organic compound (VOC) testing

To study the sensor's selectivity to VOCs, 5 μL of ethanol-water mixtures of varying compositions were brought at ~ 1 mm distance to the sensor and the response of the sensor was noted. Similar experiment was repeated with the acetone-water mixture.

Note S2. Calibration of the sensor

Sensor's response was calibrated under controlled humidity using supersaturated salt solutions in a bottle as shown in Figure S5a. Details pertaining to the quantity of salt and the corresponding humidity achieved is given below in Table S1.

Table S1. Details regarding the quantity of salt needed to create controlled humidity.

Salt name	Quantity (g)	Volume of water (mL)	Relative humidity (%RH)
LiCl	29.3	10	11
MgCl2	100	10	32.8
NaCl	41.1	10	75.3
KCl	31.2	10	84.3

Note S3. Classification of sensor data

Binary classification was implemented on the uniformly segmented dataset to classify the samples into the following categories – normal and abnormal (deep breathing and fast breathing).

The dataset was randomly split into training and test data, and four kinds of classification algorithms were applied to investigate their feasibility in detecting breathing patterns. These algorithms were chosen as they have been commonly used in machine learning in the medical field and for classifying time series.

Logistic regression was firstly used to see if treating the time series as a tabular data affected the accuracy of the classifier. Each time series was iteratively split into segments with window sizes ranging from 26 data points to 522 data points. In each iteration, features such as mean, standard deviation, maximum value, minimum value and median were extracted for every segment and a 10-fold cross validation was implemented to identify critical features. The segment size with the best cross-validation score was used to fit the classifier model.

Time series-specific classification algorithms such as Bag-of-SFA Symbols in Vector Space (BOSSVS), k-Nearest Neighbours (kNN) and Symbolic Aggregate approXimation in Vector Space Model (SAX-VSM) were also implemented with the help of the Python packages *pyts* and *pyt.* For the kNN classifier, DTW was selected as the distance metric.

Bag-of-SFA Symbols in Vector Space (BOSSVS) algorithm transform the time series and its labels into a document-term matrix format using tf-idf statistics. The time series was split into sliding windows with a window size of 48 and Symbolic Fourier Approximation (SFA) was applied to each sliding window. This transformed the time series into an unordered set of SFA words. A histogram was constructed to store the frequencies of the SFA words. For each class, a tf-idf vector was computed by using these histograms. For a new time series, the label with the highest cosine similarity between its tf vector and the tf-idf vectors of each class was chosen as the predicted class.

Symbolic Aggregate approXimation in Vector Space Model (SAX-VSM) algorithm also transforms the time series and its labels to a document-term matrix using the tf-idf statistics. First, the real-valued time series was transformed into a bag of words using Symbolic Aggregate approximation (SAX) algorithm. This algorithm reduced the time series to a Piecewise Aggregate Approximation (PAA) representation by dividing the dataset into equal-sized segments and computing the mean of the points within each segment. A window size of 36 was chosen for the segments. Then, the classes were transformed into a Vector Space Model (VSM) using term frequencies (tf) and inverse document frequencies (idf). The bag of SAX words was then transformed into a class-characteristic weight vectors using the tf-idf weighting, and these vectors were classified using the Cosine similarity. The algorithm automatically discovers and ranks time series patterns by their similarity to the label. For classifying an unlabeled time series, SAX-VSM computes cosine similarity values between the term frequency vector of the new time series and the tf-idf weight vectors representing the training classes. It is then assigned to the class whose vector yields the maximal cosine similarity value.

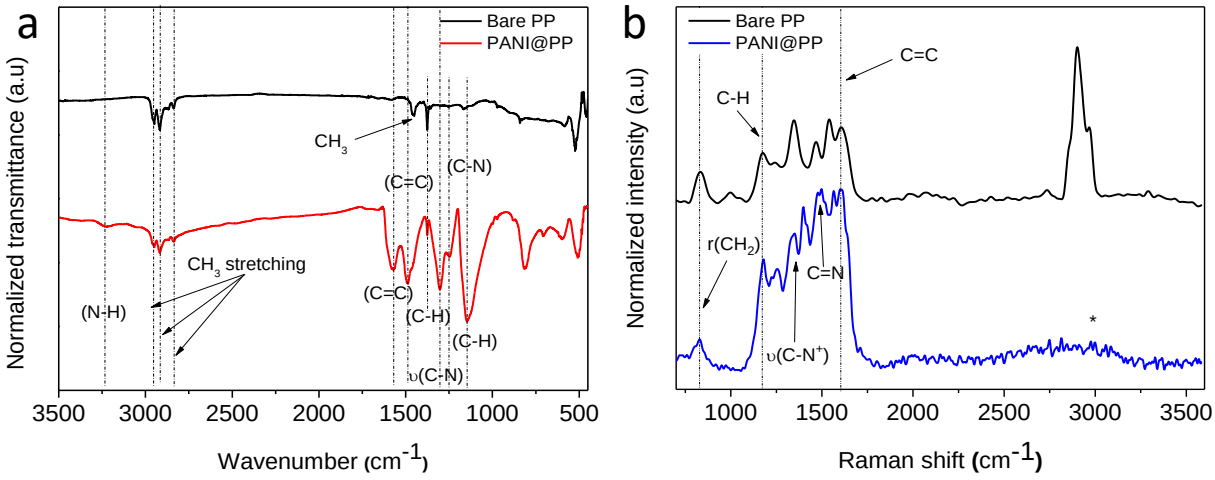

Figure S1. (a) FT-IR and (b) Raman spectrum of untreated PP and PANI@PP cloth. Prominent peaks are labeled.

Table S2. FTIR peak assignment for PP and PANI coated PP mat.

Wavenumber (cm^{-1})	PP mat	PANi@PP mat	Assignment
808	No	Yes	C-C stretching
840	Yes	No	C-H rocking[1]
1142	No	Yes	δ(C-H) stretching[2]
1161	Yes	No	(C-H) wagging[3]
1245	No	Yes	δ(C-N) stretching[4]
1303	No	Yes	γ(C-N) aromatic stretching
1379	Yes	Yes	CH_3 stretching
1456	Yes	No	CH_3 symmetric bending
1493	No	Yes	Benzoid stretching[5]
1570	No	Yes	Quinonoid ring stretching[5]
2836	Yes	Yes	CH_2 asymmetric stretching
2866	Yes	Yes	CH_3 stretching
2949	Yes	Yes	CH_3 asymmetric stretching
3230	No	Yes	γ(C-N) stretching[3]

Table S3. Raman peak assignment for PP and PANi-coated PP mat.

Raman shift (cm^{-1})	PP	PANi@PP	Assignment
829	Yes	Yes	r(CH_3)
1167	Yes	Yes	C-C stretching
1345	Yes	Yes	Graphitic disorder
1350	No	Yes	γ(C-N+) stretching
1457	Yes	Yes	δ(C-H) stretching
1489	No	Yes	γ(C=N) stretching
1500	No	Yes	δ(N-H) stretching[6]
1567	No	Yes	N-H bending
1606	Yes	Yes	C=C stretching
2818	Yes	No	γ(CH_3) symmetric stretching[7]
2966	Yes	No	γ(CH_3) asymmetric stretching[7]

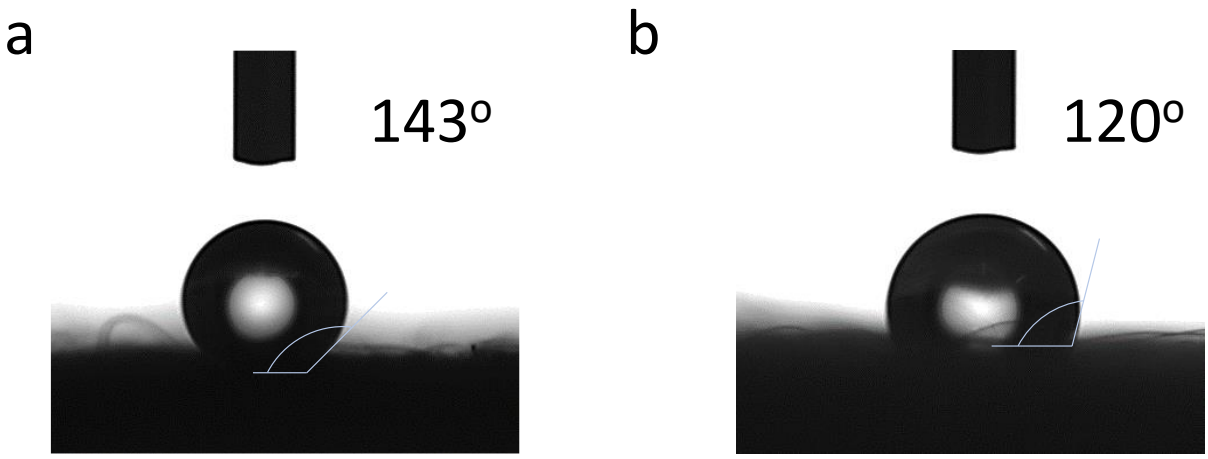

Figure S2. Contact angle measurements performed on (a) untreated PP mat, and (b) PANI@PP mat.

Table S4. Parameters obtained from the Nyquist plot.

Parameter	N_2	Room temperature	Nasal exhalation	Oral exhalation
R_s(kΩ)	2.4	2.2	1	0.63
R_{ct}(kΩ)	58	26	24	21.9
C (F)	0.87×10^{-12}	0.94×10^{-12}	3.4×10^{-12}	11.6×10^{-12}

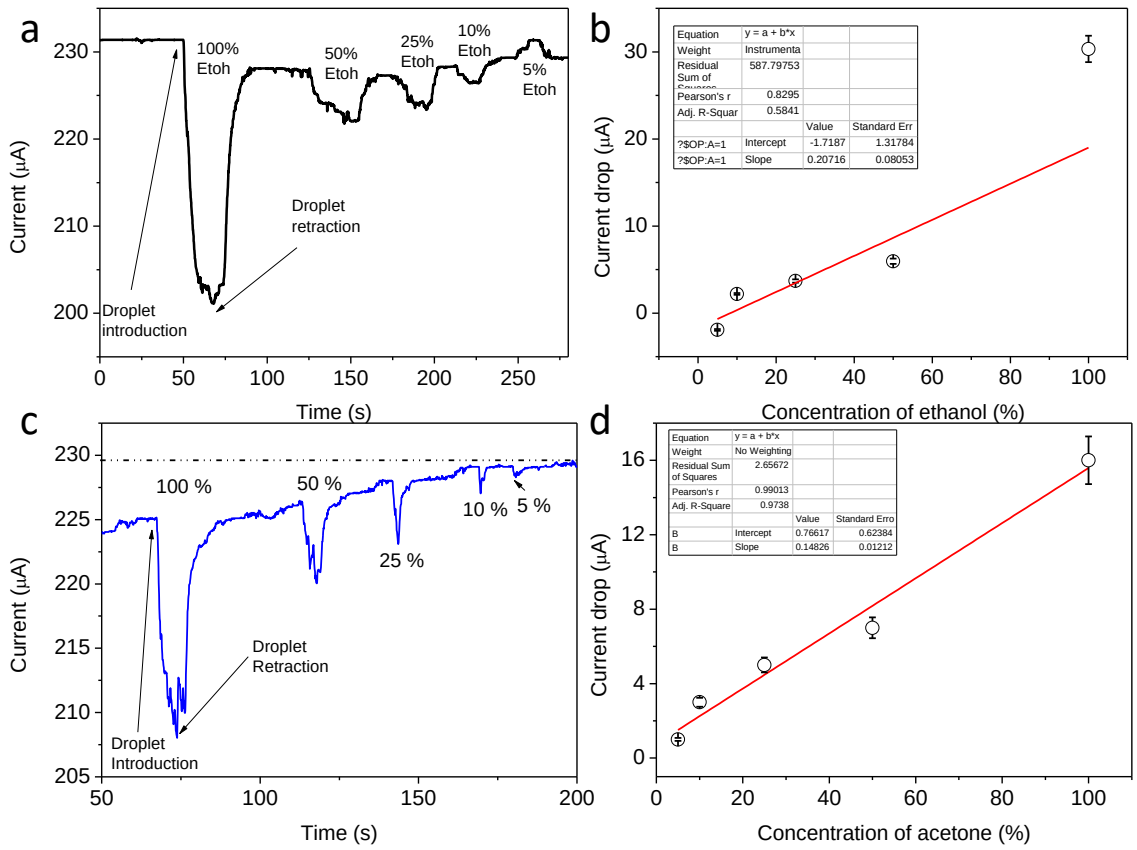

Figure S3. (a, c) Chronoamperometric response of the sensor in presence of a droplet of ethanol-water and acetone-water mixture at different concentrations. (b and d) Plot of ethanol-water and acetone-water concentrations, with respect to the current difference.

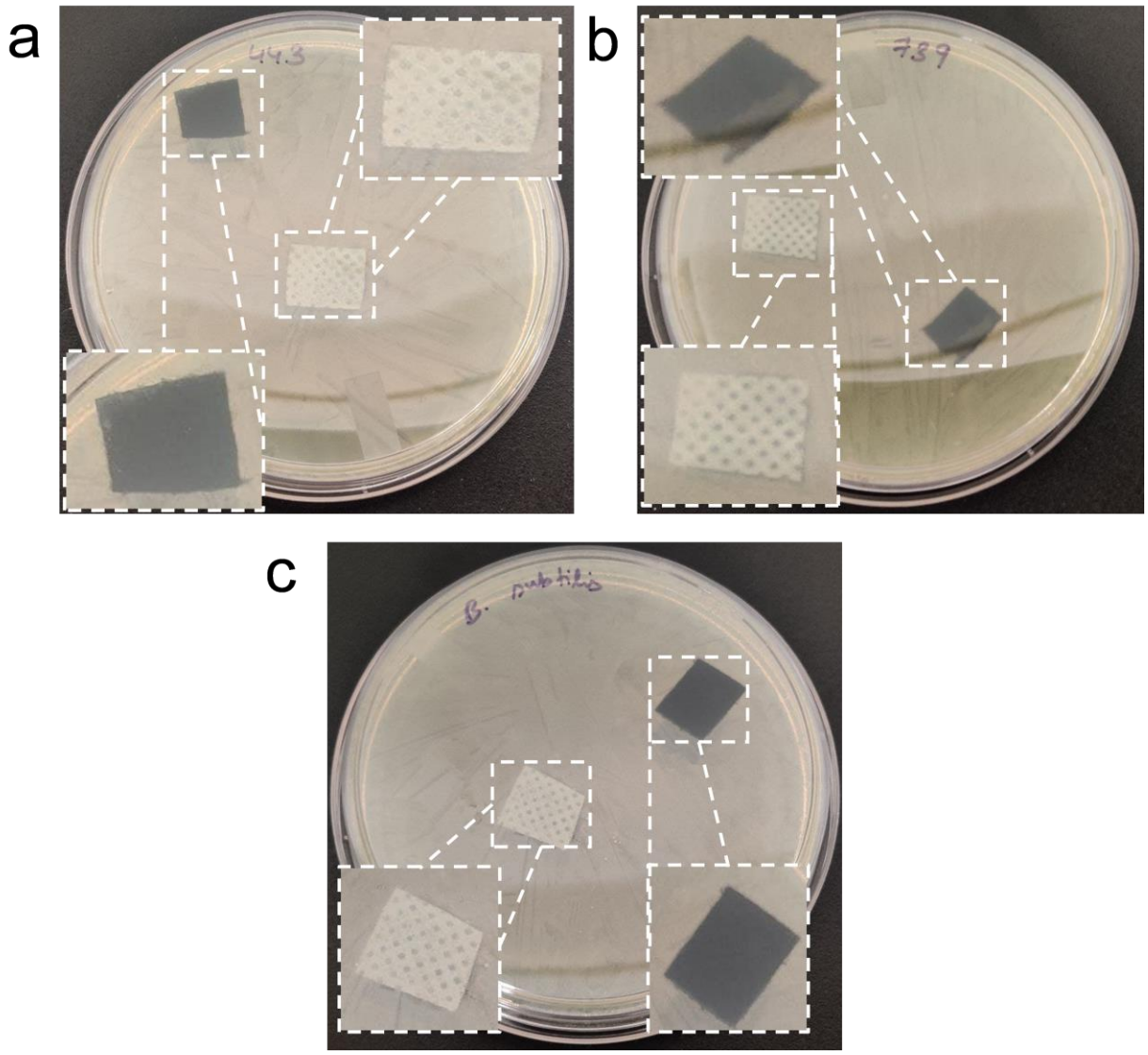

Figure S4. Testing of the antibacterial property the mats using (a) *E. coli* 443, (b) *E. coli* 739 and (c) *B. subtilis*. Here, PP and PANi@PP mats are presented in blue and green color, respectively. Magnified regions of the mats are present in the inset.

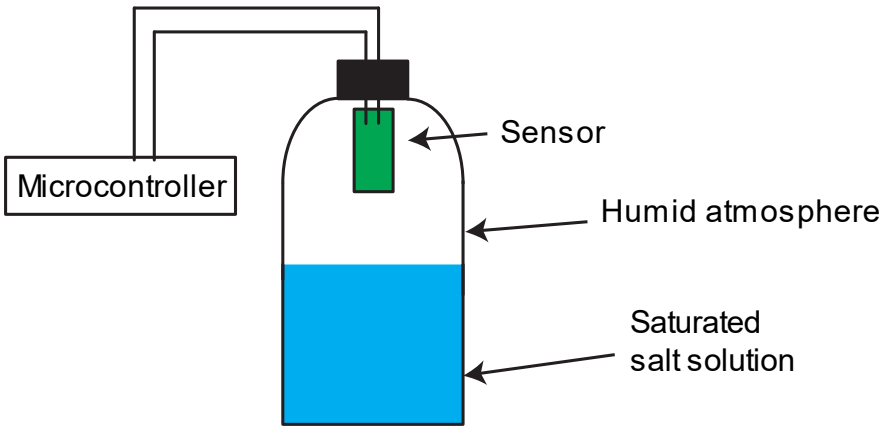

Figure S5. Schematic of the sensor calibration set-up. The microcontroller in the rectangular box represents the entire circuit system along with the microcontroller used for measuring the output voltage.

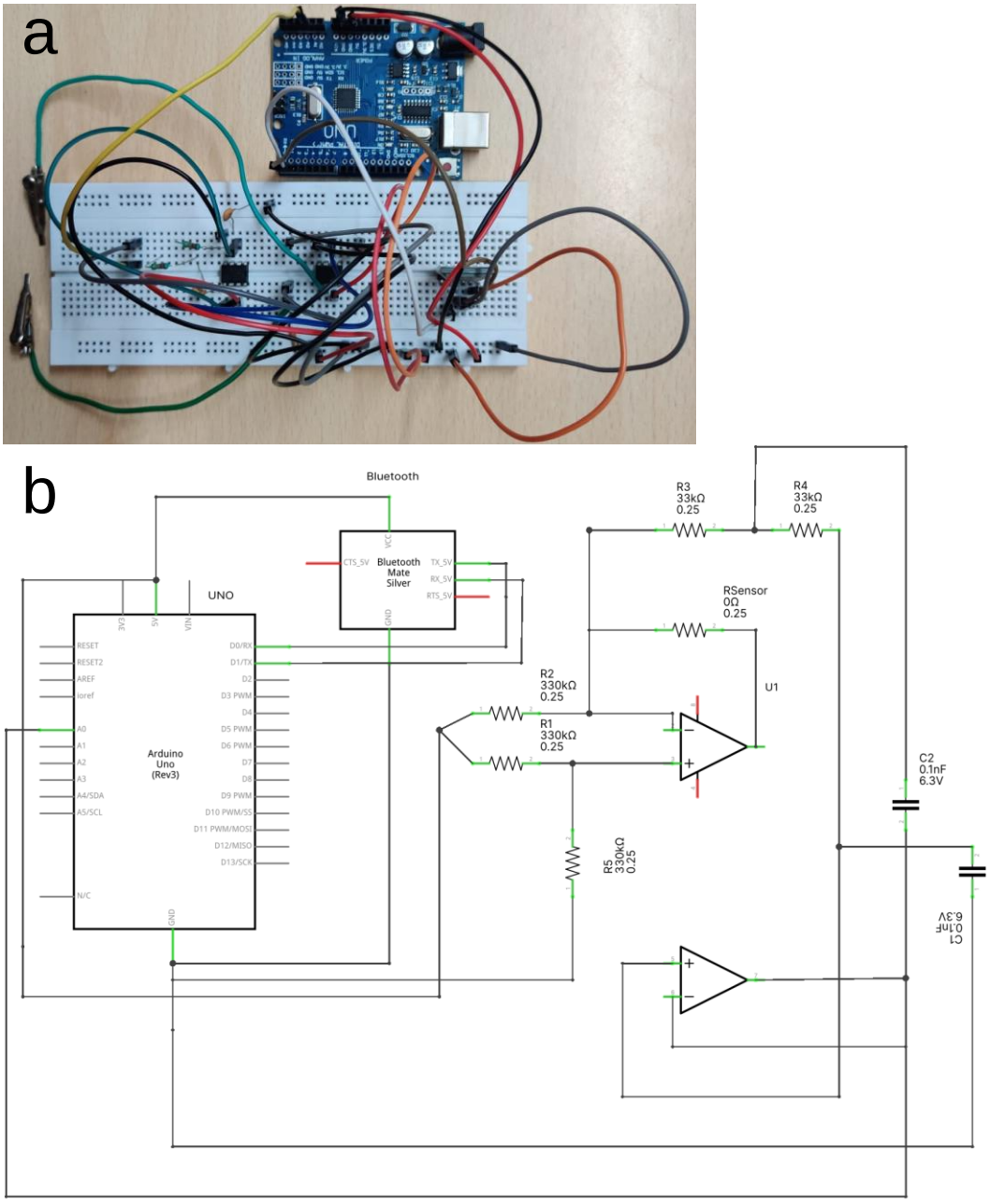

Figure S6. (a) Photograph of circuit used for measuring the humidity in the exhaled breath. (b) Schematic of the electrical circuit needed for making the entire sensing prototype.

Table S5. Bill of materials.

S.No	Component name	Cost ($)	Quantity	Overall cost ($)
1	Arduino Nano	7.54	1	7.54
2	HC-05 Bluetooth module	6.20	1	6.20
3	Male-male jumper cable	0.04	30	1.31
4	Breadboard	2	1	2
5	Resistors: 1. 330 kΩ 2. 33 kΩ	0.0078	500	3.93
6	Capacitors: 1. 0.1 μF	0.012	555	6.23
7	Conducting thread	8.22	5 m	8.22
8	Silver conductive paint	19.95	1	19.95
9	LM741 Op amp IC	0.24	10	2.48
10	Surgical mask	0.003	100	3.93
	Total for 1 smart mask	18.15	1	18.15

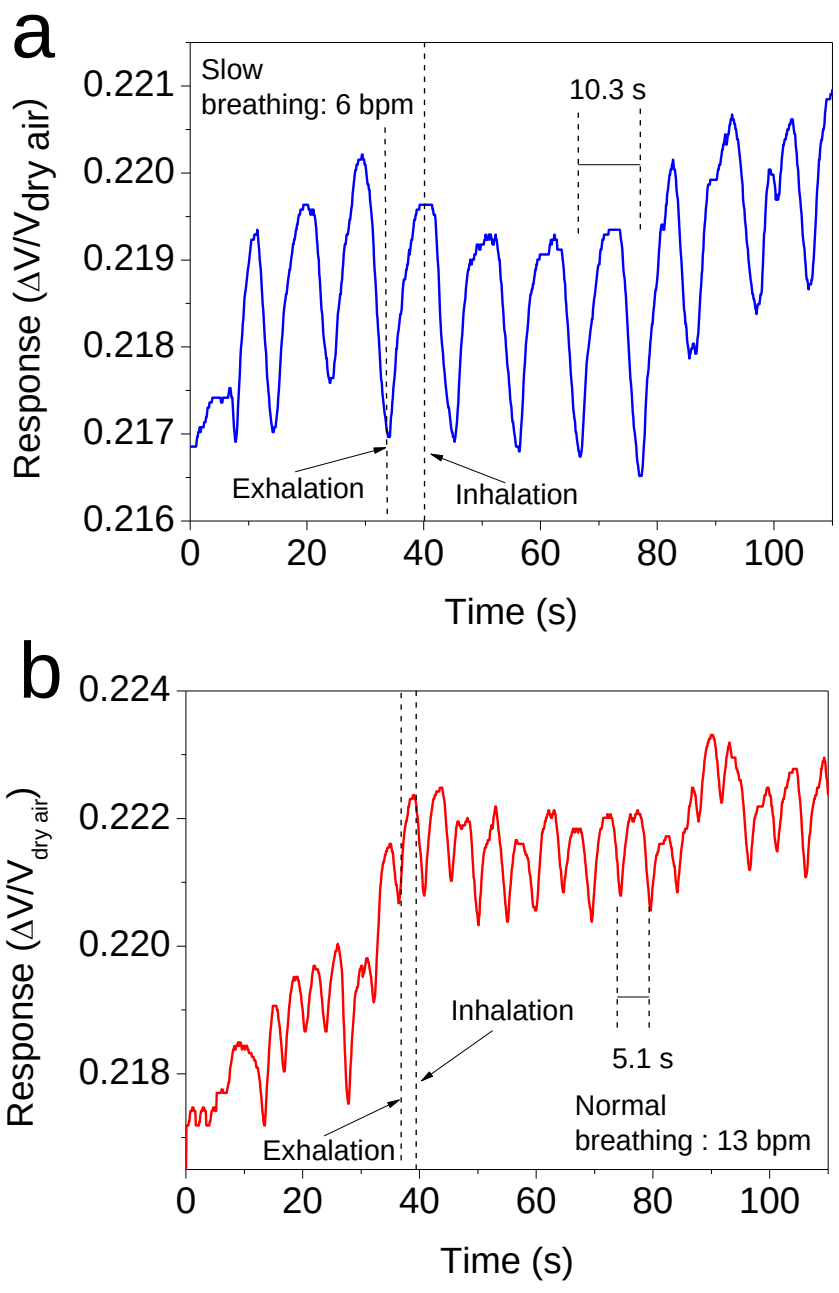

Figure S7. (a) Slow and (b) normal breathing response of an individual recorded on the mobile phone.

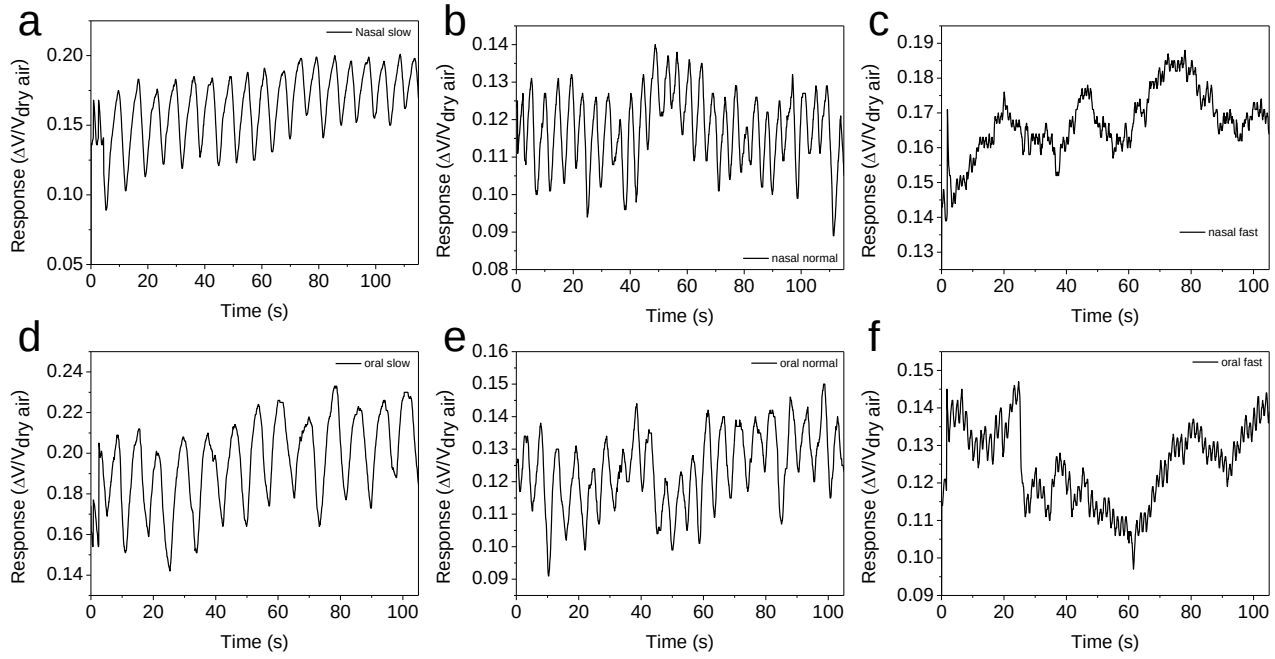

Figure S8. Breathing response from 6 different volunteers. For nasal breath: (a) slow, (b) normal and (c) fast. For oral breath: (d) slow, (e) normal and (f) fast.

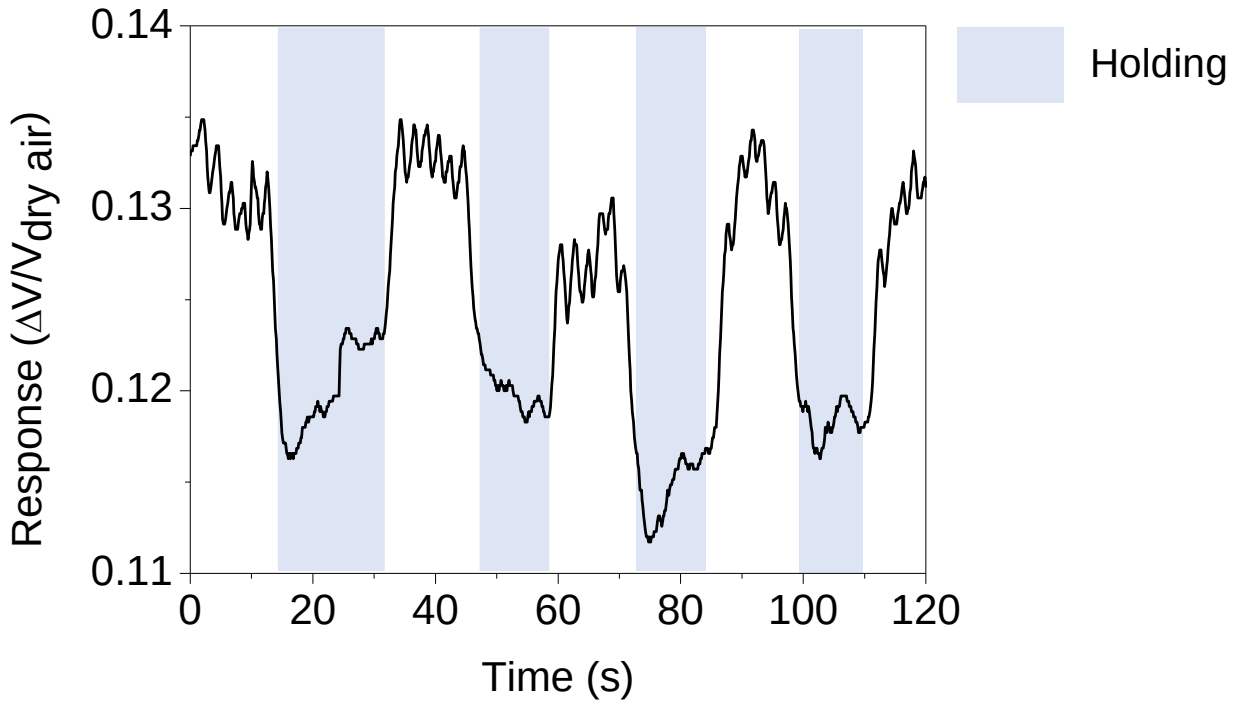

Figure S9. Sensor response for a volunteer performing a breath cycle comprising breathing and holding of breath.

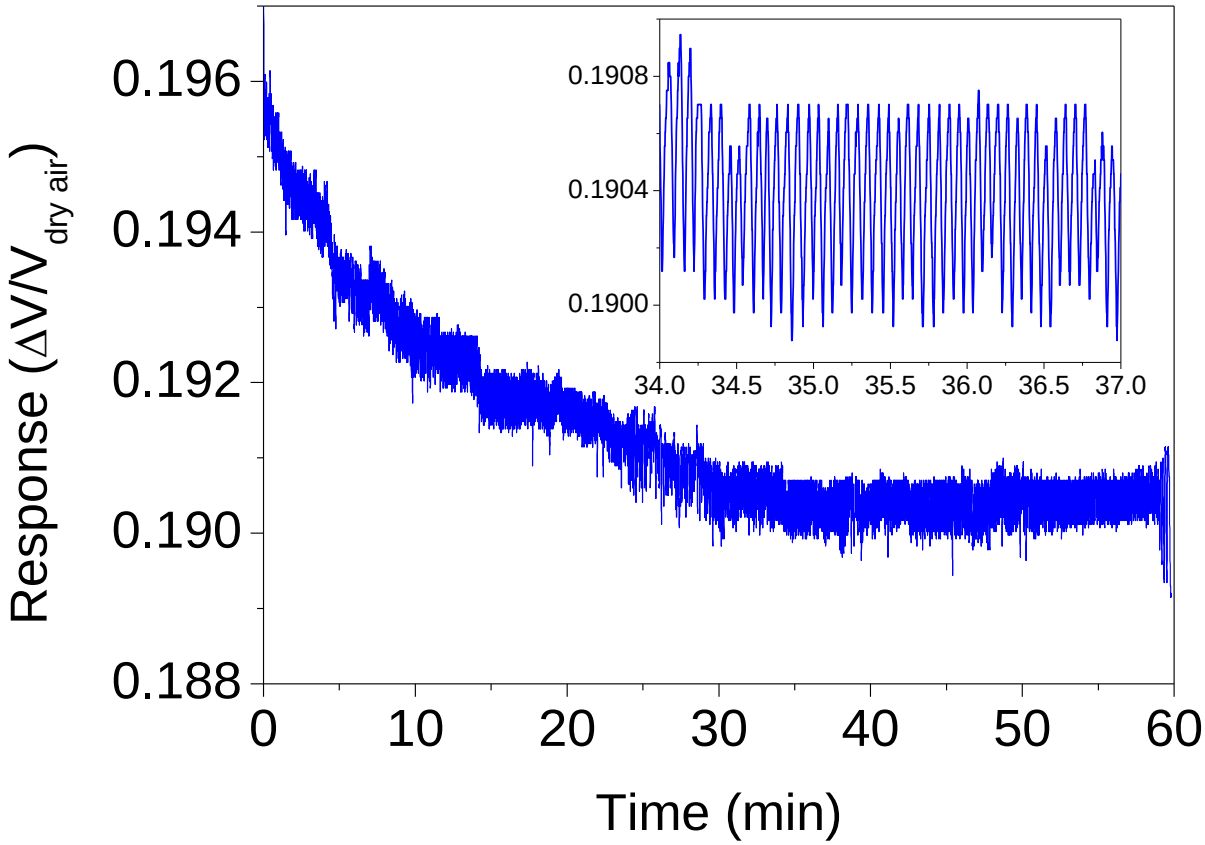

Figure S10. Breathing response of a volunteer while working. Working duration corresponds to the volunteer sitting in a comfortable position while working on his laptop. Inset shows the magnified region between 34-37 min.

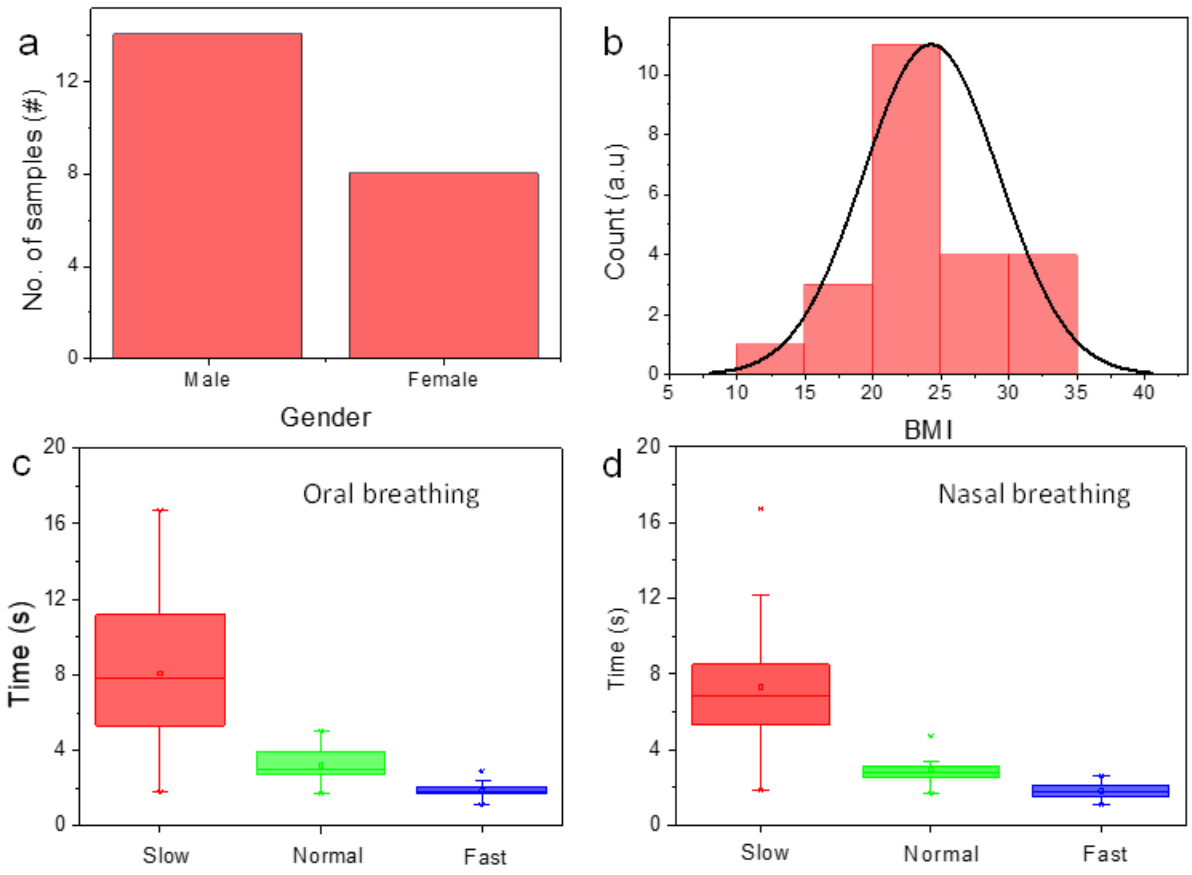

Figure S11. (a) Bar chart depicting the number of male and female volunteers in the study. (b) BMI distribution of all the volunteers. (c and d) Time required for completing a total breathing cycle orally and through the nose, respectively.

Table S6. Comparing the performance of different classifiers on the collected data.

Algorithm	Accuracy (%)	True positive rate (TPR) (%)	False Positive rate (FPR) (%)
SAX-VSM	90.42	94.64	15.79
BOSSVS	89.36	91.52	14.28
kNN	74.46	77.78	32.26
1D CNN	81.91	86.2	25
Logistic Regression	60.6	0	0

Table S7. Comparison of the properties of different humidity sensors.

Sensing material	**Response time (s)**	**Recovery Time (s)**	**Breath differentiation**	**Mobile phone integration**	**Breathing pattern classification**	**Ref**
MoSSe/PVA	~ 0.18	1.14	Yes	Yes	Yes	[8]
g-C_3N_4/TiO_2 /$Ti_3C_2T_x$	-	-	Yes	No	No	[9]
Graphene-paper	218	230	Yes	No	No	[10]
Si nano crystals	0.04	0.04	Yes	No	No	[11]
Supramolecular ionic	0.037	0.037	Yes	No	No	[12]

material (SIM)						
Graphene oxide-modified PDA	0.02	0.017	Yes	Yes	No	[13]
Natural polymer sphere QCM	-	-	Yes	Yes	No	[14]
ACNT@PU fibers	-	-	Yes	No	No	[15]
Fabric@GO@BSA	8.9	11.6	Yes	No	No	[16]
1T/2H-MoS_2 nanoparticles	76	382	Yes	No	No	[17]
Laser induced graphene	63	8	Yes	No	No	[18]
GO/Li-doped GO /B-doped GO	23	4	No	No	No	[19]
PANi@PP	1.2	2.8	Yes	Yes	Yes	This work

References

(1) Fang, J.; Zhang, L.; Sutton, D.; Wang, X.; Lin, T. Needleless Melt-Electrospinning of Polypropylene Nanofibres. *J. Nanomater.* **2012**, *2012*, e382639. https://doi.org/10.1155/2012/382639.

(2) *Infrared and Raman Characteristic Group Frequencies: Tables and Charts, 3rd Edition | Wiley*. Wiley.com. https://www.wiley.com/en-us/Infrared+and+Raman+Characteristic+Group+Frequencies%3A+Tables+and+Charts%2C+3rd+Edition-p-9780470093078 (accessed 2022-05-19).

(3) Kang, E. T.; Neoh, K. G.; Tan, K. L. Polyaniline: A Polymer with Many Interesting Intrinsic Redox States. *Prog. Polym. Sci.* **1998**, *23* (2), 277–324. https://doi.org/10.1016/S0079-6700(97)00030-0.

(4) Trchová, M.; Stejskal, J. Polyaniline: The Infrared Spectroscopy of Conducting Polymer Nanotubes (IUPAC Technical Report). *Pure Appl. Chem.* **2011**, *83* (10), 1803–1817. https://doi.org/10.1351/PAC-REP-10-02-01.

(5) *Vibrational Analysis of Polyaniline: A Model Compound Approach | The Journal of Physical Chemistry B*. https://pubs.acs.org/doi/10.1021/jp972652o (accessed 2021-08-18).

(6) Trchová, M.; Morávková, Z.; Bláha, M.; Stejskal, J. Raman Spectroscopy of Polyaniline and Oligoaniline Thin Films. *Electrochimica Acta* **2014**, *122*, 28–38. https://doi.org/10.1016/j.electacta.2013.10.133.

(7) Andreassen, E. Infrared and Raman Spectroscopy of Polypropylene. In *Polypropylene: An A-Z reference*; Karger-Kocsis, J., Ed.; Polymer Science and Technology Series; Springer Netherlands: Dordrecht, 1999; pp 320–328. https://doi.org/10.1007/978-94-011-4421-6_46.

(8) Bokka, N.; Karhade, J.; Sahatiya, P. Deep Learning Enabled Classification of Real-Time Respiration Signals Acquired by MoSSe Quantum Dot-Based Flexible Sensors. *J. Mater. Chem. B* **2021**, *9* (34), 6870–6880. https://doi.org/10.1039/D1TB01237A.

(9) Guo, X.; Kuang, D.; Zhu, Z.; Ding, Y.; Ge, L.; Wu, Z.; Du, B.; Liang, C.; Meng, G.; He, Y. Humidity Sensing by Graphitic Carbon Nitride Nanosheet/TiO2 Nanoparticle/Ti3C2Tx

Nanosheet Composites for Monitoring Respiration and Evaluating the Waxing of Fruits. *ACS Appl. Nano Mater.* **2021**, *4* (10), 11159–11167. https://doi.org/10.1021/acsanm.1c02625.

(10) Liu, H.; Zheng, H.; Xiang, H.; Wang, W.; Wu, H.; Li, Z.; Zhuang, J.; Zhou, H. Paper-Based Wearable Sensors for Humidity and VOC Detection. *ACS Sustain. Chem. Eng.* **2021**, *9* (50), 16937–16945. https://doi.org/10.1021/acssuschemeng.1c05156.

(11) Kano, S.; Kim, K.; Fujii, M. Fast-Response and Flexible Nanocrystal-Based Humidity Sensor for Monitoring Human Respiration and Water Evaporation on Skin. *ACS Sens.* **2017**, *2* (6), 828–833. https://doi.org/10.1021/acssensors.7b00199.

(12) Yan, H.; Zhang, L.; Yu, P.; Mao, L. Sensitive and Fast Humidity Sensor Based on A Redox Conducting Supramolecular Ionic Material for Respiration Monitoring. *Anal. Chem.* **2017**, *89* (1), 996–1001. https://doi.org/10.1021/acs.analchem.6b04350.

(13) He, J.; Xiao, P.; Shi, J.; Liang, Y.; Lu, W.; Chen, Y.; Wang, W.; Théato, P.; Kuo, S.-W.; Chen, T. High Performance Humidity Fluctuation Sensor for Wearable Devices via a Bioinspired Atomic-Precise Tunable Graphene-Polymer Heterogeneous Sensing Junction. *Chem. Mater.* **2018**, *30* (13), 4343–4354. https://doi.org/10.1021/acs.chemmater.8b01587.

(14) Yang, J.; Feng, L.; Chen, Y.; Feng, L.; Lu, J.; Du, L.; Guo, J.; Cheng, Z.; Shi, Z.; Zhao, L. High-Sensitivity and Environmentally Friendly Humidity Sensors Deposited with Recyclable Green Microspheres for Wireless Monitoring. *ACS Appl. Mater. Interfaces* **2022**. https://doi.org/10.1021/acsami.2c00489.

(15) Huang, X.; Li, B.; Wang, L.; Lai, X.; Xue, H.; Gao, J. Superhydrophilic, Underwater Superoleophobic, and Highly Stretchable Humidity and Chemical Vapor Sensors for

Human Breath Detection. *ACS Appl. Mater. Interfaces* **2019**, *11* (27), 24533–24543. https://doi.org/10.1021/acsami.9b04304.

(16) Wang, Y.; Zhang, L.; Zhang, Z.; Sun, P.; Chen, H. High-Sensitivity Wearable and Flexible Humidity Sensor Based on Graphene Oxide/Non-Woven Fabric for Respiration Monitoring. *Langmuir* **2020**, *36* (32), 9443–9448. https://doi.org/10.1021/acs.langmuir.0c01315.

(17) Taufik, A.; Asakura, Y.; Hasegawa, T.; Kato, H.; Kakihana, M.; Hirata, S.; Inada, M.; Yin, S. Surface Engineering of 1T/2H-MoS2 Nanoparticles by O2 Plasma Irradiation as a Potential Humidity Sensor for Breathing and Skin Monitoring Applications. *ACS Appl. Nano Mater.* **2020**, *3* (8), 7835–7846. https://doi.org/10.1021/acsanm.0c01352.

(18) Zou, S.; Tao, L.-Q.; Wang, G.; Zhu, C.; Peng, Z.; Sun, H.; Li, Y.; Wei, Y.; Ren, T.-L. Humidity-Based Human–Machine Interaction System for Healthcare Applications. *ACS Appl. Mater. Interfaces* **2022**, *14* (10), 12606–12616. https://doi.org/10.1021/acsami.1c23725.

(19) Rathi, K.; Pal, K. Impact of Doping on GO: Fast Response–Recovery Humidity Sensor. *ACS Omega* **2017**, *2* (3), 842–851. https://doi.org/10.1021/acsomega.6b00399.